Multi-Actuator Full-Scale Fatigue Test of a Tidal Blade

Sergio. Lopez Dubon, Christopher. Vogel, David. Garcia Cava, Fergus. Cuthill, Edward D. McCarthy and Conchur M. Ó Bradaigh

Abstract*—Tidal stream energy is a rapidly growing industry that faces many challenges, including the mechanical testing of very stiff composite material blades. Among the mechanical tests, fatigue testing is particularly challenging. It is not possible to test tidal turbine blades at their natural frequencies (ca. 18-20 Hz), as is done for wind blades, because tidal blades have much higher natural frequencies, and hydraulic test technology cannot achieve resonant testing at these high frequencies. It is then required to apply loads using an external system (commonly a hydraulic system) at a frequency that avoids thermal failures due to heating. Nevertheless, traditional hydraulic systems cannot (in most cases) apply high loads at high frequencies. Moreover, conventional hydraulic systems tend to be inefficient during a fatigue test since the energy used to the blade is lost after the end of each cycle. Under this scenario, the FastBlade facility was developed to help the tidal energy industry to test composite tidal blades. FastBlade features a regenerative digital displacement hydraulic pump system that allows it to recover up to 75% of the energy (compared to a traditional hydraulic system) in each cycle. To demonstrate FastBlade's test performance, we developed a real case scenario in which loads were computed from Reynolds-Averaged Navier Stokes simulations based on measured water velocity profiles and later replicated by FastBlade using three actuator points. Tests were conducted at different load frequencies and percentages of the maximum root bending moment, similar to those the blade may experience under normal environmental conditions. A series of measurements were taken, showing the behaviour of the blade at different locations.

Keywords*— Testing, Fatigue, Tidal Steam Blades, Composites.

I. INTRODUCTION

TIDAL and wave energy sources have the potential to generate 100GW for the EU power grid by 2050, contributing to a third of EU homes and adding economic activity and jobs [1]. Horizontal axis turbines (HATs) are crucial for the growth of tidal stream energy. However, designing HATs is challenging as they operate in seawater, which is 800 times denser than air, and requires managing significantly higher loads per unit blade span. Current designs of tidal turbine blades based on blade element momentum theory and simplified Finite Element Models are given [2-4]. Due to the high fluid stresses, tidal turbine blades have high-stress concentrations, which increase the risk of fatigue failure over a 20-year design life. The lack of data and understanding of fatigue in tidal blades results in structurally conservative blade designs and high levelized costs of energy (LCOE) compared to other renewable energy technologies [5]. To reduce turbine blade fatigue failure risk and lower the LCOE, there is a renewed focus on improved test methods, more representative data, and new design methodologies.

Recent advances in full-scale fatigue testing of composite material tidal blades include a 2018 test at the University of Galway, where a 3/8th scale blade design by OpenHydro was tested, achieving a maximum load

Sponsor and financial support acknowledgement: First Author: This project have received funding from the European Union's Horizon 2020 research and innovation programme under the Marie Skłodowska-Curie grant agreement No 801215 and the University of Edinburgh Data-Driven Innovation programme, part of the Edinburgh and South East Scotland City Region Deal.

All authors: The authors also wish to thank the Supergen ORE Hub for funding received through the Flexible Fund Award FF2020-1063.

Sergio Lopez Dubon is with the School of Engineering, The University of Edinburgh, Scotland, United Kingdom. (e-mail: Sergio.LDubon@ed.ac.uk).

Christopher Vogel is with the Department of Engineering Science, University of Oxford, Oxford, England, United Kingdom. (e-mail: christopher.vogel@eng.ox.ac.uk).

David. Garcia Cava is with the School of Engineering, The University of Edinburgh, Scotland, United Kingdom. (e-mail: david.garcia@ed.ac.uk).

Fergus Cuthill is with the School of Engineering, The University of Edinburgh, Scotland, United Kingdom. (e-mail: fergus.cuthill@ed.ac.uk).

Edward D. McCarthy is with the School of Engineering, The University of Edinburgh, Scotland, United Kingdom. (e-mail: ed.mccarthy@ed.ac.uk).

Conchur M. Ó Bradaigh is with the School of Engineering, The University of Edinburgh, Scotland, United Kingdom. (e-mail: c.obradaigh@ed.ac.uk).

Digital Object Identifier: https://doi.org/10.36688/ewtec-2023-177

amplitude of 35kN and 275,000 cycles [6]. In 2020, a new turbine blade fatigue test standard was published, IEC TS 62600-3:2020 [7], and in 2022, the new FastBlade facility at Port of Rosyth, Scotland, was opened, which can deliver accelerated lifetime fatigue testing of a full-scale tidal blade and other long slender structures [8]. In the same year, at the University of Galway, another fatigue test was performed with two full-scale blades of 2 and 3 metres in length from SCHOTTEL HYDRO, achieving a maximum load of 6.9 kN during 150,000 cycles at 0.3Hz for the 2-metre blade, and a maximum load of 14 kN during 16,000 cycles at 0.1Hz for the 3-metre blade [9]. Moreover, the latter authors also performed a three-actuator test for static at high load following the standard IEC TS 62600-3:2020. This was followed by fatigue testing at low load and an increased number of cycles up to 300,000 following the standard DNVGL-ST-0164 [10] and a final static test [11]. In 2022, the first high load fatigue test reaching an RBM (Root Bending Moment) of 652 kN.m and high-frequency 1Hz was performed at FastBlade following the standard IEC TS 62600-3:2020 . The test performed 31,775 cycles, equivalent to 21.7 years of tides. The blade did not suffer any catastrophic failure or significant changes in stiffness [12-13]. In this study, we explore the use of 3 actuators and the response of the blade to different frequencies going from 0.1 up to 1.5 Hz. The blade used in this study is the same as that used in the FastBlade tests in 2022 [12-13].

II. DATA AND METHODS

A. Site Data

This project utilised flow data sourced from the ReDAPT project, conducted at the Fall of Warness, European Marine Energy Centre (EMEC), Orkney, UK [14-16]. The data were collected using two acoustic Doppler current profilers positioned 0.8 m above the seabed between July 19th and August 2nd, 2013. The profilers sampled the flow at a frequency of 0.5 Hz, with a mean operating depth of 43.2 m and 46.2 m due to slightly different seabed conditions at their locations.

To analyse the data, the flow speed and turbulence intensity values were grouped into hub-height mean flow speed bins of U_∞=(0.7,1.4,2.1,2.8,3.0,3.5) $m.s^{-1}$ for both flood and ebb tides, with the highest value of U_∞=3.5 $m\ s^{-1}$ achieved only during ebb tide. Measurements were included only when the wave height was less than 1 metre to ensure data quality. A 5-minute ensemble length was employed for all statistics, and a turbulence intensity noise correction estimate of 0.12 $cm.s^{-1}$ was applied by the procedure outlined in [15].

B. Fluid dynamic computational model

The computational fluid dynamics (CFD) solver OpenFOAM (version 2.3.1) was utilised to perform a series of unsteady Reynolds-Averaged Navier Stokes (URANS) simulations. The choice of URANS simulation is based on the work of [17], who found that URANS and Large Eddy Simulation produce similar phase-averaged loads and blade pressure distributions in low onset turbulence flows (focus of this paper). The PimpleFoam PISO algorithm was used for the simulations, with the turbulence closure provided by the k-ω SST model utilising the 2003 updated coefficients [18]. Each simulation was run for 400s, with a time step of 0.03s.

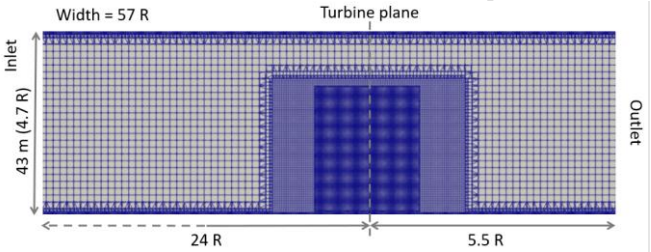

Figure 1. Octree mesh used in the CFD.

The computational domain utilised in this study spanned 250 metres in length, 520 metres in width, and 43 metres in height, which matched the height of the ReDAPT site. The domain width was set to achieve a small geometric blockage ratio of 1.14%, with a vertical flow profile imposed at the inlet of the computational domain utilising the atmospheric boundary layer inlet condition available in OpenFOAM. The flow profile was sustained by a no-slip wall boundary condition at the bottom of the domain and a stress boundary condition at the top. A fixed static pressure of 0 Pa was established at the outlet boundary, and zero gradient boundary conditions were applied to the turbulence and velocity scalars. Symmetry conditions were employed at the lateral boundaries of the domain. The inflow and top boundary conditions were tailored to match the observed flow profile from the ReDAPT data.

The study used an Octree mesh with three levels of grid refinement to discretise the computational domain. The mesh parameters were evaluated for convergence and agreed with field observations using a homogeneous grid dimension of 1.5 m. Two additional levels of refinement were employed near the rotor and in the wake region, resulting in a mesh with approximately 2.8×10^6 elements. The actuator line method was used to represent representedliminating the need for rotating sub-domains or mesh interfaces and reducing computational costs. However, the mesh was refined close to the turbine to capture the large velocity gradients around the blades (see Fig 1).

The actuator line method of [19] was used to represent the turbine blades, with each blade represented by a rotating line along which force is applied to the flow [20-21]. Blade forces were calculated using 2D blade element theory at 100 collocation points. The flow field around each blade was sampled using the potential flow equivalence method and reimposed using the Gaussian smearing technique. The calculated blade forces were modified by the tip loss model of Shen et al. [22] to emulate the 3D flow, which reduce the blade forces near

the tips. The turbine nacelle was represented using a cell-blocking method to enforce zero velocity and allow impermeable bodies to be represented in the numerical domain without explicit geometry resolution [23]. The model has been validated against reference turbines.

C. *Blade Data*

The blade (see Fig 2) was designed by Tidal Generation Limited and manufactured by Aviation Enterprises Limited as part of the DeepGen tidal project. The blade was taken from a decommissioned 500kW tidal stream turbine installed at EMEC's test site at the Fall of Warness. Some design documents were lost and not provided to FastBlade before testing. The company responsible for the blade design no longer exists; another company bought the rights (Airborne).

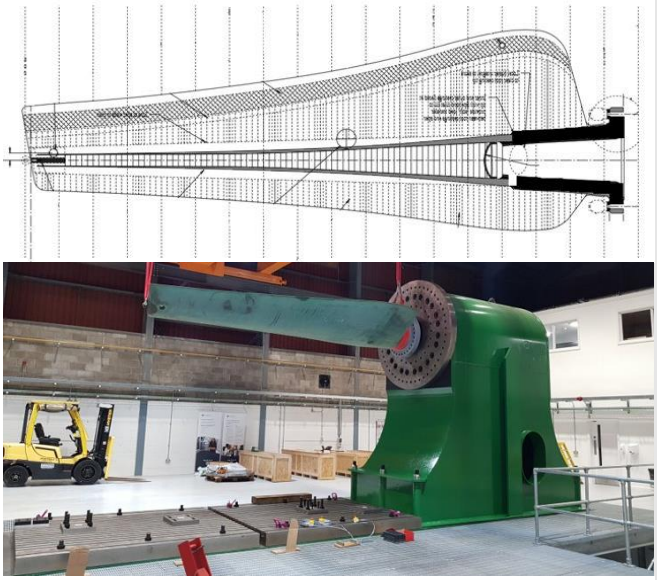

Figure 2. Technical Drawing of the Test Blade Looking from the Top View [25] and the original blade [12-13].

The blade's cross-section is based on the NACA 63-4XX aerofoil series, where XX represents the thickness-to-chord ratio varying from 55% at the root to 18% at the tip. The innermost part of the blade had a cylindrical cross-section with an implied thickness-to-chord ratio of 100%. The aerofoil lift and drag characteristics as a function of the angle of attack were computed using QBlade with a chord-based Reynolds number range of $1.0 \times 10^7 < Re < 1.8 \times 10^7$ and a critical number $N_{crit} = 9$ for all cases. NACA aerofoil coordinates were determined [24] using 300 equally spaced points.

The blade is covered with an 8mm thick glass fibre skin, and pairs of 3 mm thick glass fibre ribs are used to stiffen it. The spar cap comprises 75% unidirectional carbon fibre epoxy prepreg with shear webs made of ±45° carbon fibre epoxy prepreg. A rear glass fibre epoxy spar connects the suction and pressure sides 100mm away from the trailing edge to relieve the trailing edge joint from peel stresses. [26]. The blade had been tested before at FastBlade using one actuator following the IEC TS 62600-3:2020 [7]. From these previous tests, it is known that the blade's centre of gravity is 900 ± 30 mm from the root, and the weight of the blade is 1588.59 kg (15584.07 N). The natural frequency tests showed a slight reduction of 0.54% from 18.0278 Hz to 17.9308 Hz at the end of the test campaign, which suggests minor damage [27].

III. EXPERIMENT

With the target load defined, a test campaign using 3 rams or actuators in which the same load was applied to each of them was performed. The test campaign consists of 33 fatigue tests of 100 cycles each, following Table 1.

TABLE 1
LIST OF EXPERIMENTS CARRIED OUT

Test No.	Frequency [Hz]	% of max Load [kN/kN]	Offset [kN]	Amplitude [kN]	Max Load Per Ram [kN]	Min Load Per Ram [kN]
1	0.1	51%	20.48	12.8	33.28	7.68
1b	0.1	40%	16	10	26	6
2	0.1	60%	24	15	39	9
3	0.1	80%	32	20	52	12
4	0.1	100%	40	25	65	15
5	0.3	40%	16	10	26	6
6	0.3	60%	24	15	39	9
7	0.3	80%	32	20	52	12
8	0.3	100%	40	25	65	15
9	0.5	40%	16	10	26	6
10	0.5	60%	24	15	39	9
11	0.5	80%	32	20	52	12
12	0.5	100%	40	25	65	15
13	0.7	40%	16	10	26	6
14	0.7	60%	24	15	39	9
15	0.7	80%	32	20	52	12
16	0.7	100%	40	25	65	15
17	0.9	40%	16	10	26	6
18	0.9	60%	24	15	39	9
19	0.9	80%	32	20	52	12
20	0.9	100%	40	25	65	15
21	1.1	40%	16	10	26	6
22	1.1	60%	24	15	39	9
23	1.1	80%	32	20	52	12
24	1.1	100%	40	25	65	15
25	1.3	40%	16	10	26	6
26	1.3	60%	24	15	39	9
27	1.3	80%	32	20	52	12
28	1.3	100%	40	25	65	15
29	1.5	40%	16	10	26	6
30	1.5	60%	24	15	39	9
31	1.5	80%	32	20	52	12
32	1.5	100%	40	25	65	15

A. *FastBlade Facility Description*

FastBlade is equipped with a 70-tonne reaction frame that can withstand high loads during both static and fatigue testing, as indicated in Table 2. Additionally, it has a reversible hydraulic flow of 880 litres per minute.

TABLE 2
FASTBLADE CAPABILITIES [12-13]

Load Capacity	Moment [MN-m]	Shear [MN]
FATIGUE (Up to 400 million cycles pushing)	4.70	0.94
FATIGUE (Up to 400 million cycles Pulling)	4.70	0.94
STATIC (Assuming quasi-static loading Pulling)	11.96	2.39
STATIC (Assuming quasi-static loading Pushing)	10.74	2.13

The FastBlade frame consists of a reaction plane, support wall, T-Slot bed plates, and adapter plate. It is mounted on bridge bearings and located in a 2.5 m deep pit on the floor (see Fig 3). The FastBlade hydraulic system uses four Digital Displacement hydraulic reversible pumps developed by Danfoss, allowing the system to recover the energy used during testing. This system operates with up to 75% less energy consumption than similar-sized hydraulic systems and provides control of the actuators, allowing for the implementation of compound loads that can better represent complex ocean interactions.

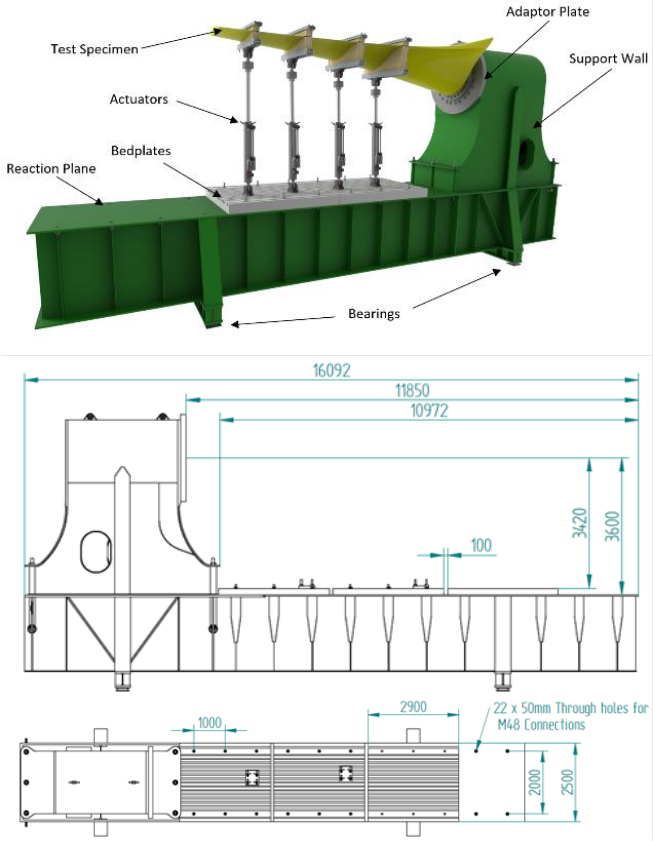

Figure 3. FastBlade reaction frame configuration [12-13].

B. *Set up and data collection.*

The FastBlade system includes a reaction frame, hydraulic system, and data collection system. The hydraulic system uses four Digital Displacement hydraulic reverse pumps to recover the energy used during the test and can operate with up to 75% less energy than similar hydraulic systems. The data collection system uses various sensors, including load cells, accelerometers, linear position sensors, strain gauges, thermocouples, and linear string potentiometers, and it is controlled by Flex-logger software. This paper reports data from the strain gages and displacement sensors, which are located along line one in the horizontal direction (x-axis) for the top and bottom part of the blade, as shown in Figure 4.

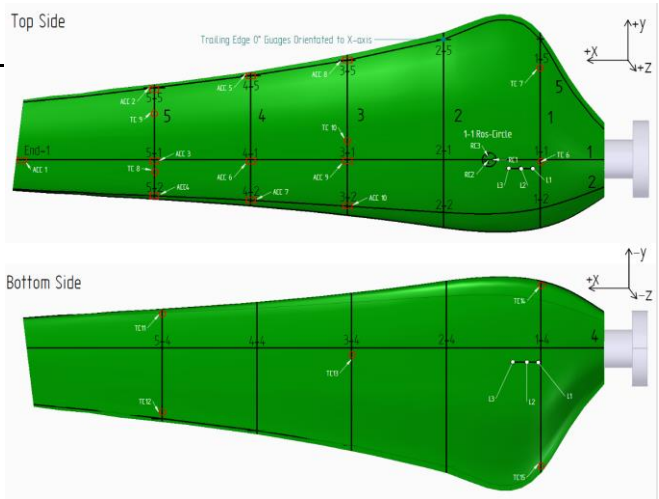

Figure 4. Sensor location on the top and bottom of the blade.

The loading direction for the test was determined based on [26], and three actuators located at 2.2751, 3.5600, and 4.4770 metres from the back face of the blade connection flange, pushing in the XBB direction, were identified as the optimal loading location achieving the moment about the YBB axis, as shown in Figure 5. The blade was also monitored using Digital Image Correlation (DIC) equipment.

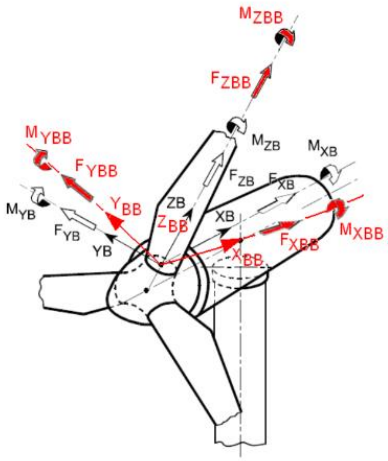

Figure 5 Blades coordinate system [12-13].

A series of clamped wooden saddles with a surrounding steel frame and a 1.5 mm thick silicone sheet at the blade interface introduced the loads. The induced stresses applied to the blade due to the clamping system are still under analysis. Nevertheless, preliminary results from the DIC system suggest they are negligible in relation to the stresses due to the loads. The final system configuration can be appreciated in Figure 6.

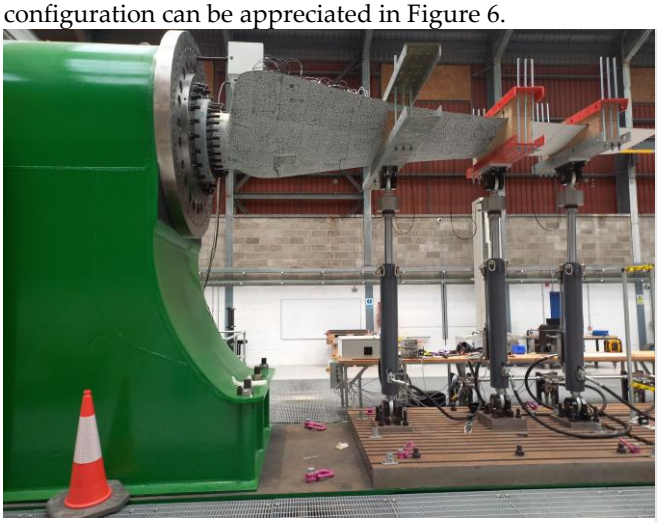

Figure 6. FastBlade reaction frame test setup with 3 actuators.

IV. RESULTS

A. Simulated Loads

The study simulated the rotor at different flow speeds during flood and ebb tides. The rotor performed differently due to the variation in velocity shear profiles between the tides, even at the same hub-height velocity. The spanwise axial and tangential blade loads were analysed, and generally increased along the blade due to the increasing incident flow speed, see Fig 7. The mean blade loads were slightly higher for the rotor in the ebb tide due to a more significant velocity shear across the rotor swept area. These factors caused the rotor to operate further from its hydrodynamic optimum, resulting in increased minimum-maximum spread in blade loads, particularly in the lower part of the rotation.

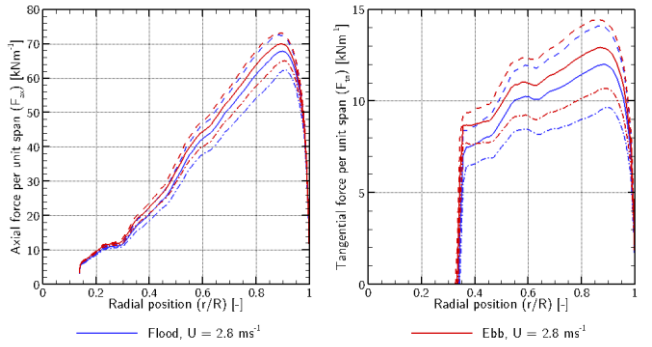

Figure 7 The axial (on the left) and tangential (on the right) blade loads along the span for both flood (in blue) and ebb (in red) tides at a flow speed of 2.8 ms-1. The solid line represents the mean load during a rotation, while dashed and dash-dot lines are used to indicate the minimum and maximum loads, respectively [13].

The simulations showed that the blade loads, overall power, and thrust fluctuated due to rotational sampling of the shear profile by the blades, resulting in azimuthal variations in blade root bending moments. Normalised RBMs were higher for the rotor operating in the ebb tide between 90-270°. However, the higher flood RBMs countered this in the upper half of the blade rotation (see Fig 8). The relative variation in the edgewise RBMs was more remarkable due to sensitivity to the angle of attack of the flow onto the blade. The maximum and minimum RBMs occurred at slightly different azimuthal positions from the top and bottom-dead centre due to the interaction between rotor-induced swirl velocity and shear profile.

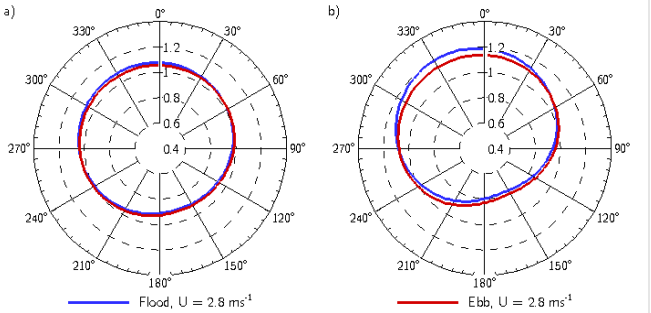

Figure 8. Normalized blade root bending moments in the flapwise (left) and edgewise (right) directions are shown for the flood (blue) and ebb (red) tides, operating at a hub-height flow speed of U=2.8 ms-1, indicating the azimuthal variation [13].

B. Fatigue test

After obtaining hydrodynamic results, the collected ocean data was extrapolated for one year using harmonic analysis. This enabled the identification of the prevailing bending moment at the root, with a magnitude of 652 kN.m, following the Table 1 scheme. Due to the number of sensors and data generated, just a few of them are presented in the current work; we present RBM, the loads on each actuator, and the displacement at the tip.

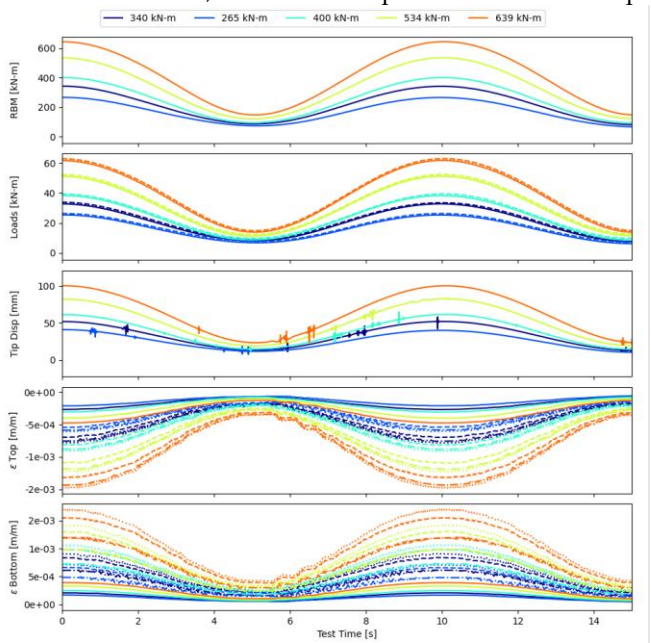

Figure 9. Data of the first 1.5 cycles for tests No 1 to 4 (see Table 1) with a frequency of 0.1 Hz.

Moreover, we selected a few strain gauges, all measuring in the x direction (see Fig. 4); for the top area of the blade, we reported the data for positions 1_1, 2_1, 3_1 and 4_1 and for the bottom of the blade 1_4, 2_4, 3_4 and 5_4 (all positions in reference to Fig 4), represented as solid, dashed, dotted, and dash-dot lines.

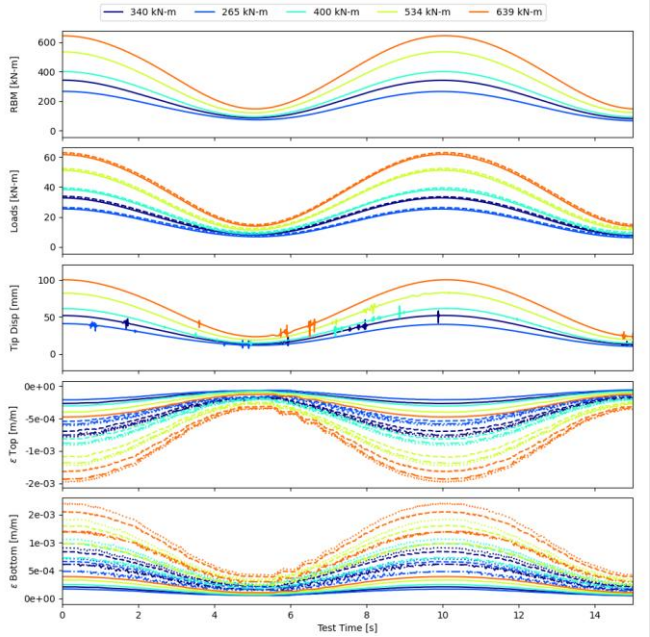

Figure 9. Data of the first 1.5 cycles for tests No 1 to 4 (see Table 1) with a frequency of 0.1 Hz.

The first set of tests can be seen in Fig 9, where a series of low frequency at different loads tests were performed from Test No 1 to Test No 4 refer to Table 1. In this figure, the first one-and-a-half cycle is shown. The values of the strains are relatively symmetric, with higher values on the bottom of the blade, as can be seen in Table 4.

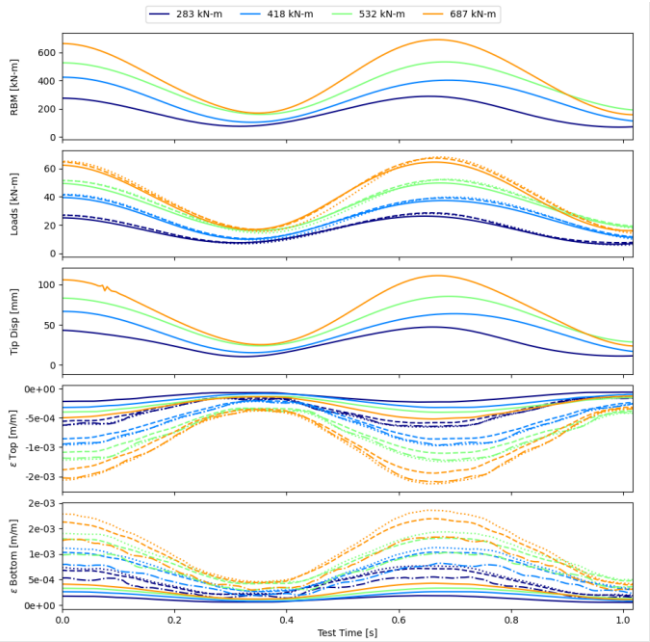

Figure 10. Data of the first 1.5 cycles for tests No 29 to 32 (see Table 1) with a frequency of 1.5 Hz.

In Fig. 10, we present the data from the test performed at 1.5 Hz; the data show a similar trend as the data from Fig 8, as Tables 3 and 4 confirm. This confirms that the blade can be tested at a high frequency and that similar results are obtained to those obtained when performing the same test at a low frequency.

Figure 11 shows the results for all the tests at the lower load and for a time equal to 1.5 half cycles of the slowest frequency test. It can be seen that the range of displacement and strain gauges values remain relatively similar.

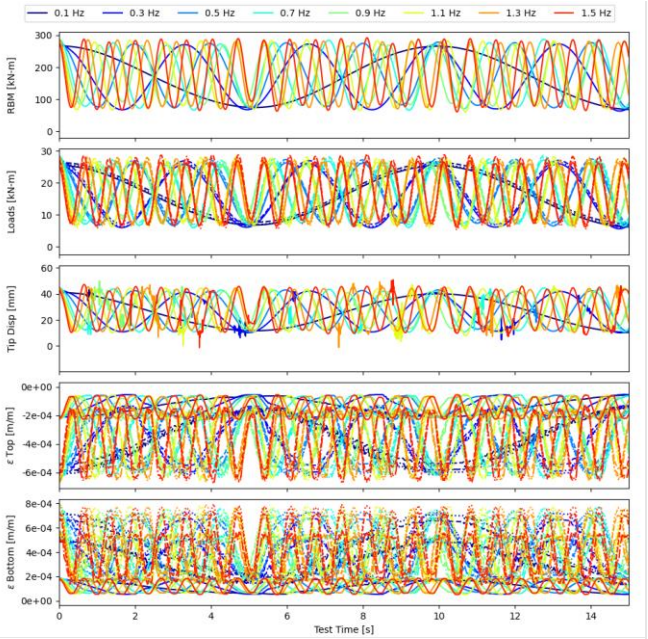

Figure 11. Data of Tests No. 1b, 5, 9, 13, 17, 21, 25 and 29 (see Table 1) for minimum loads.

Figure 12 shows the results for all the tests at the higher load and for a time equal to 1.5 half cycles of the slowest frequency. This graph is aligned with all the previous ones, with the difference that noise due to the control system response is lower than Fig 11.

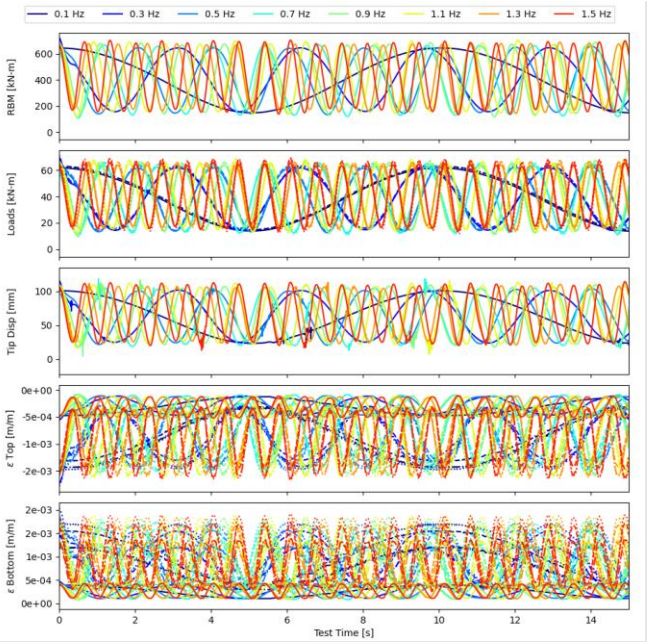

Figure 11. Data of Tests No. 4, 8, 12, 16, 20, 24, 28 and 32 (see Table 1) for maximum loads.

TABLE 3
MEAN DISPLACEMENT AT PEAK CYCLE PER TEST

Test No	RBM [kN.m]	Centre [mm]	Tip [mm]	Act_01 [mm]	Act_02 [mm]	Act_03 [mm]
1	341	10	52	6	19	37
1b	266	7	40	4	15	28
2	401	11	62	7	22	43
3	534	15	83	9	30	58
4	640	18	100	11	36	70
5	272	7	42	5	15	29
6	407	11	63	7	23	44
7	541	15	84	9	31	58
8	643	18	101	11	36	69
9	274	7	42	5	15	29
10	411	11	64	7	23	44
11	544	15	85	10	31	59
12	649	18	102	11	37	70
13	280	8	43	5	16	30
14	415	12	65	7	23	45
15	547	15	86	10	31	60
16	662	19	104	12	38	72
17	271	7	42	5	15	29
18	416	12	65	7	23	45
19	552	16	87	10	31	60
20	676	19	107	12	39	74
21	281	8	44	5	16	31
22	422	12	66	8	24	46
23	560	16	88	10	32	61
24	683	19	108	12	39	76
25	280	8	44	5	16	31
26	420	12	66	7	24	46
27	558	16	88	10	32	61
28	675	19	107	12	39	75
29	284	8	45	5	16	31
30	419	12	66	8	24	46
31	533	15	85	10	30	59
32	687	20	110	12	40	77

Act stands for actuator.

From the data of Table 3, if we compute the ratio of displacement against RBM, the relation remains constant for the first significant value and with low changes on the second significant value (i.e., for tests 01 and 02, the relation of central displacement against RMB is 0.0028 and for test 31 and 32 this relation is 0.0029). Similar behaviour can be seen in Fig 13 where for the peak of each cycle for tests No. 4, 8, 12, 16, 20, 24, 28 and 32 (see Table 1) the tip displacements is located against the RBM. This demonstrates that the Fasblade facility can manage different test loads and frequencies, and, most importantly, any possible damage during these tests can be considered negligible.

Table 4 shows the results of the mean strain values

TABLE 4
MEAN STRAIN AT PEAK CYCLE PER TEST

Test No	1_1 [ε]	2_1 [ε]	3_1 [ε]	4_1 [ε]	1_4 [ε]	2_4 [ε]	3_4 [ε]	5_4 [ε]
1	-3	-7	-8	-8	2	8	9	6
1b	-2	-5	-6	-6	2	7	7	5
2	-3	-8	-9	-9	3	10	11	7
3	-4	-11	-12	-12	3	13	14	10
4	-5	-13	-15	-14	4	15	17	12
5	-2	-5	-6	-6	2	7	7	5
6	-3	-8	-9	-9	3	10	11	8
7	-4	-11	-12	-12	3	13	14	10
8	-5	-13	-15	-14	4	15	17	12
9	-2	-5	-6	-6	2	7	7	5
10	-3	-8	-9	-9	3	10	11	8
11	-4	-11	-12	-12	3	13	14	10
12	-5	-13	-15	-14	4	16	17	12
13	-2	-6	-6	-6	2	7	8	5
14	-3	-8	-9	-9	3	10	11	8
15	-4	-11	-13	-12	3	13	15	10
16	-5	-13	-15	-15	4	16	17	12
17	-2	-6	-6	-6	2	7	7	5
18	-3	-9	-10	-9	3	10	11	8
19	-4	-11	-13	-12	3	14	15	10
20	-5	-14	-16	-15	4	16	18	13
21	-2	-6	-6	-6	2	7	8	5
22	-3	-9	-10	-9	3	10	11	8
23	-4	-12	-13	-13	3	14	15	11
24	-5	-14	-16	-16	4	17	18	13
25	-2	-6	-6	-6	2	7	8	5
26	-3	-9	-10	-9	3	10	11	8
27	-4	-12	-13	-13	3	14	15	11
28	-5	-14	-16	-16	4	16	18	13
29	-2	-6	-6	-6	2	7	8	5
30	-3	-9	-10	-10	3	10	11	8
31	-4	-11	-12	-12	3	13	14	10
32	-5	-14	-16	-16	4	17	19	13

All the values have to be multiplied by 10E-4

with a resolution of 1.0E-3. The table shows how the bottom and top of the blade show similar behaviour (tension–compression); as in the case of Table 3, the mean strain values remain relatively constant regardless of the frequency, and they depend just on the load. Moreover, can appreciate a reduction in the strain values when they move from 2_1 and 2_4 to 1_1 and 1_4, respectively; this behaviour is in concordance with the structure of the blade (see section C).

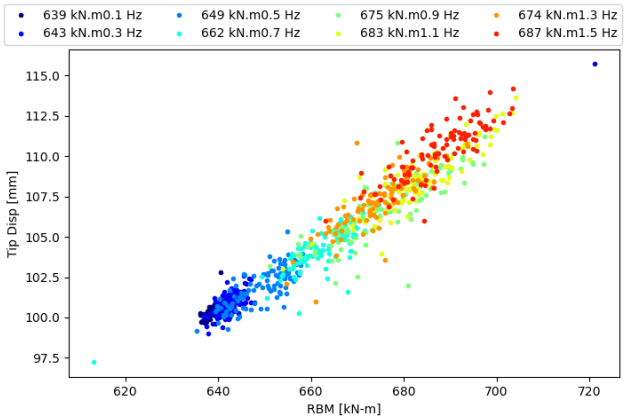

Figure 13. RBM vs tip displacement at top of each cycle of Tests No. 4, 8, 12, 16, 20, 24, 28 and 32 (see Table 1).

V. CONCLUSIONS

In this work, we demonstrate the ability of FastBlade to perform a series of mechanical fatigue tests at different frequencies and loads. For each load and frequency, 100 cycles were performed to ensure the reproducibility of the test and to ensure the system could repeat the same loads at the same frequency. From this test series, a series of valuable lessons for FastBlade and the blade industry can be drawn.

It was shown that FastBlade performs accurate control regarding if it runs at higher loads and regardless of the different frequencies tested. These tests allow us to improve the FastBlade control system to manage different frequencies.

The blade showed a similar mechanical response regardless of the test frequency; this finding reinforces the position of FastBlade as a facility for accelerated fatigue testing. During all the tests, the blade remained with a similar relation between displacement and total root bending moment, which suggests that the blade did not suffer any significant damage during these tests.

VI. REFERENCES

[1] H. Jeffrey, S. Pennock, JLVillate, P Ruiz-Minguela, D. Cagney, L. Pirttimaa, A European Ocean Energy Industry – the €140bn Economic Opportunity, Industrial Roadmap for Ocean Energy, (n.d.). https://www.etipocean.eu/knowledge_hub/industrial-roadmap-for-ocean-energy/ (accessed January 13, 2023).

[2] D.M. Grogan, S.B. Leen, C.R. Kennedy, C.M. Ó Brádaigh, Design of composite tidal turbine blades, Renew. Energy. 57 (2013) 151–162. https://doi.org/10.1016/j.renene.2013.01.021.

[3] C.R. Kennedy, S.B. Leen, C.M.. M.M.. Brádaigh, A preliminary design methodology for fatigue life prediction of polymer composites for tidal turbine blades, Proc. Inst. Mech. Eng. Part L J. Mater. Des. Appl. 226 (2012) 203–218. https://doi.org/10.1177/1464420712443330.

[4] C.R. Kennedy, V. Jaksic, S.B. Leen, C.M.Ó. Brádaigh, Fatigue life of pitch- and stall-regulated composite tidal turbine blades, Renew. Energy. 121 (2018) 688–699. https://doi.org/10.1016/j.renene.2018.01.085.

[5] A. S. Evans, Analysis: Record-low price for UK offshore wind is nine times cheaper than gas - Carbon Brief, (n.d.). https://www.carbonbrief.org/analysis-record-low-price-for-uk-offshore-wind-is-four-times-cheaper-than-gas/ (accessed January 13, 2023).

[6] O. de la Torre, D. Moore, D. Gavigan, J. Goggins, Accelerated life testing study of a novel tidal turbine blade attachment, Int. J. Fatigue. 114 (2018) 226–237. https://doi.org/10.1016/J.IJFATIGUE.2018.05.029.

[7] British Standards Institution, Marine energy. Wave, tidal and other water current converters. Part 3, Measurement of mechanical loads., British Standards Institution, 2020. https://www.document-center.com/standards/show/PD-IEC-62600-3 (accessed January 13, 2023).

[8] F.R. Cuthill, J.R. Steynor, S.L. Dubon, E.D. Mccarthy, C. Conch´, C.M.´ Brádaigh, J.R. Steynor Is Senior, E.D. Mccarthy, Development of the world's first regenerative hydraulic tidal blade test centre: FASTBLADE, in: Eur. Wave Tidal Energy Conf. 14th EWTEC, Plymouth, 2021. https://proceedings.ewtec.org/product/ewtec-2021-plymouth-uk/ (accessed January 13, 2023).

[9] C. Glennon, W. Finnegan, N. Kaufmann, · Patrick Meier, Y. Jiang, R. Starzmann, J. Goggins, Tidal stream to mainstream: mechanical testing of composite tidal stream blades to de-risk operational design life, J. Ocean Eng. Mar. Energy. 8 (2022) 163–182. https://doi.org/10.1007/s40722-022-00223-4.

[10] DNV, GL. Tidal turbines. DNV Standard. DNVGL-ST-0164. Oslo, Norway, 2015. https://www.dnv.com/energy/standards-guidelines/dnv-st-0164-tidal-turbines.html

[11] William Finnegan, Yadong Jiang, Patrick Meier, Le Chi Hung, Edward Fagan, Finlay Wallace, Conor Glennon, Michael Flanagan, Tomas Flanagan, Jamie Goggins, Numerical modelling, manufacture and structural testing of a full-scale 1 MW tidal turbine blade, Ocean Engineering, Volume 266, Part 1, 2022, 112717, ISSN 0029-8018, https://doi.org/10.1016/j.oceaneng.2022.112717.

[12] Lopez Dubon, Sergio Antonio and Vogel, Christopher R. and García Cava, David and Cuthill, Fergus and McCarthy, Edward D. and Ó Bradaigh, Conchur M., Fastblade: A Technological Facility for Full-Scale Tidal Blade Fatigue Testing. Available at SSRN: https://ssrn.com/abstract=4400928 or http://dx.doi.org/10.2139/ssrn.4400928

[13] Lopez Dubon, Sergio Antonio and Vogel, Christopher R. and García Cava, David and Cuthill, Fergus and McCarthy, Edward D. and Ó Bradaigh, Conchur M., Fastblade: A Technological Facility for Full-Scale Tidal Blade, SAMPE 2023, Seattle, WA, USA http://dx.doi.org/ 10.33599/nasampe/s.23.0062

[14] B. Sellar, Metocean Data Set from the ReDAPT Tidal Project: Batch 1, Part 2, 2011-2014, (2017). https://doi.org/https://doi.org/10.7488/ds/1687.

[15] B.G. Sellar, TIDAL ENERGY SITE CHARACTERISATION AT THE FALL OF WARNESS, EMEC, UK, Edinburgh, 2016. https://redapt.eng.ed.ac.uk/library/eti/reports_updated/Technical Report on Tidal Site Characaterisation During the ReDAPT Project v4.0.pdf.

[16] B.G. Sellar, G. Wakelam, D.R.J. Sutherland, D.M.I. Id, V. Venugopal, Characterisation of Tidal Flows at the European Marine Energy Centre in the Absence of Ocean Waves, Energies. 11 (2018). https://doi.org/10.3390/en11010176.

[17] U. Ahmed, D.D. Apsley, I. Afgan, T. Stallard, P.K. Stansby, Fluctuating loads on a tidal turbine due to velocity shear and turbulence: Comparison of CFD with field data, Renew. Energy. 112 (2017) 235–246. https://doi.org/10.1016/J.RENENE.2017.05.048.

[18] F.R. Menter, M. Kuntz, R. Langtry, Ten Years of Industrial Experience with the SST Turbulence Model, Turbul. Heat Mass Transf. 4. (2003). http://aaac.larc.nasa.gov/tsab/cfdlarc/aiaa-dpw/ (accessed January 13, 2023).

[19] J.N. Sørensen, W.Z. Shen, Numerical Modeling of Wind Turbine Wakes, J. Fluids Eng. 124 (2002) 393–399. https://doi.org/10.1115/1.1471361.

[20] J. Schluntz, R.H.J. Willden, An actuator line method with novel blade flow field coupling based on potential flow equivalence,

Wind Energy. 18 (2015) 1469–1485. https://doi.org/10.1002/we.1770.

[21] A. Wimshurst, R.H.J. Willden, Analysis of a tip correction factor for horizontal axis turbines, Wind Energy. 20 (2017) 1515–1528. https://doi.org/10.1002/WE.2106.

[22] W.Z. Shen, J.N. Sørensen, R. Mikkelsen, Tip Loss Correction for Actuator/Navier–Stokes Computations, J. Sol. Energy Eng. 127 (2005) 209–213. https://doi.org/10.1115/1.1850488.

[23] D.D. Apsley, T. Stallard, P.K. Stansby, Actuator-line CFD modelling of tidal-stream turbines in arrays, J. Ocean Eng. Mar. Energy. 4 (2018) 259–271. https://doi.org/10.1007/S40722-018-0120-3/FIGURES/17.

[24] C. L. Larson, C.W. Brooks, A.S.H. Jr, D.W. Sproles., Computer program to obtain ordinates for NACA airfoils. Tech Report 4741, Hampton, Virginia, USA, 1996. https://ntrs.nasa.gov/api/citations/19970008124/downloads/19970008124.pdf.

[25] C. Huxley-Reynard, J. Thake, G. Gibberd, TG-RE-040-0091 Rev B Deepgen Blade Design Report, Bristol, 2008.

[26] C. Huxley-Reynard, J. King, G. Gibberd, TG-RE-000-0081 Rev D Extreme and Fatigue Load Calculations for Deepgen 500kW Tidal Turbine, Bristol, 2008.

[27] I Negru, G R Gillich, Z I Praisach, M Tufoi and N Gillich, Natural frequency changes due to damage in composite beams, Journal of Physics: Conference Series, Volume 628, 11th International Conference on Damage Assessment of Structures (DAMAS 2015) 24–26 August 2015, Ghent, Belgium, DOI 10.1088/1742-6596/628/1/012091